PCCP

PAPER

Cite this: *Phys. Chem. Chem. Phys.*, 2018, **20**, 1964

Optimal pathways for the assembly of the Apaf-1·cytochrome *c* complex into apoptosome

Hong Qi,[ab] Yu Jiang,[c] Zhiyong Yin,[c] Ke Jiang,[c] Linxi Li[c] and Jianwei Shuai*[cd]

Received 1st October 2017,
Accepted 12th December 2017

DOI: 10.1039/c7cp06726g

rsc.li/pccp

The formation of a heptameric apoptosome is a crucial event in the intrinsic cell death pathway. Considerable progress has been made towards unraveling the constituents and the structure of the apoptosome as well as the mechanism of apoptosome-mediated caspase-9 activation. However, a significant gap remains in the understanding of this process, *i.e.*, how seven Apaf-1·cytochrome *c* complexes stepwisely assemble into an apoptosome. Here, we construct a biophysical model that incorporates current biochemical knowledge about the formation of apoptosome. We propose 11 elementary routes and enumerate all 2047 possible assembly pathways from the Apaf-1·cytochrome *c* complex to the heptameric apoptosome. By combining mathematical analysis and numerical simulation, we find that two elementary routes are the most favorable biochemical reaction routes and there are 52 optimal assembly pathways which are economical and relatively fast. Our study yields the first comprehensive analysis of apoptosome assembly and provides insights into complex assembly pathways.

1 Introduction

Apoptosis is a mode of cell death that is involved in normal development and homeostasis of multicellular organisms.[1,2] In vertebrates, apoptosis proceeds through one of the two signaling cascades termed as the extrinsic and intrinsic pathways.[2,3] In the intrinsic pathway, cytochrome *c* is released from the mitochondria into the cytosol.[3,4] Once in the cytoplasm, it induces oligomerization of apoptotic protease-activating factor 1 (Apaf-1) in the presence of dATP or ATP, forming a heptameric wheel-like signaling platform dubbed apoptosome.[5,6] This platform recruits and activates initiator caspase 9, which, in turn, cleaves and activates executioner caspases, caspase 3 and caspase 7.[2] The executioners degrade several hundred proteins that ultimately cause cell death.[1,7]

The assembly of the heptameric apoptosome, therefore, represents a pivotal step in the intrinsic pathway of apoptosis. Intensive research in the last couple of decades has revealed a wealth of detail on the apoptosome components (including cytochrome *c*, Apaf-1, and dATP or ATP),[8–10] the structural information of apoptosome,[11–13] and the mechanism of apoptosome-mediated caspase-9 activation.[7,14,15] It is well known that the formation of apoptosome is a multistep process.[16] In the first step, cytochrome *c* binds to Apaf-1, forming the Apaf-1·cytochrome *c* (AC) complex. In the final step, seven AC complexes assemble into a larger and organized heptamer, *i.e.*, apoptosome. However, there is a paucity of information concerning how the heptamers are generated with individual AC complexes.

Nakabayashi and Sasaki constructed a mathematical model for the assembly process of apoptosome, in which they assumed that the oligomer composed of i molecules of AC can interact with the oligomer composed of j molecules of AC when $i+j$ is less than 7.[17] Models by Harrington *et al.*[18] and Wurstle and Rehm[19] used the same assumption. Ryu *et al.* posited that the heptameric apoptosome is assembled by adding AC one by one.[20] In general, we propose that the assembly pathways should be far more than these two schemes. Furthermore, we also believe that the biological assembly pathways should be the optimal process regarding the utilization rate and the assembly time.

In this work, we develop a biophysical model to describe the formation of the AC complex and the stepwise assembly of the apoptosome. We compare all 2047 possible pathways from seven molecules of AC to assemble an apoptosome, and obtain 52 economical and fast pathways as the optimal ones, which fits well with experimental data. To our knowledge, this is the first comprehensive analysis of apoptosome assembly. Our scheme may also provide insights into how high-order aggregates, such as amyloid and inflammasome, are assembled optimally.

2 Model and methods

Integrating the available biological information, we propose a model for apoptosome formation, which consists of three

[a] *Complex Systems Research Center, Shanxi University, Taiyuan 030006, China*
[b] *Shanxi Key Laboratory of Mathematical Techniques and Big Data Analysis on Disease Control and Prevention, Shanxi University, Taiyuan 030006, China*
[c] *Physics Department, Xiamen University, Xiamen 361005, China*
[d] *State Key Laboratory of Cellular Stress Biology, Innovation Center for Cell Signaling Network, Xiamen University, Xiamen, 361102, China. E-mail: jianweishuai@xmu.edu.cn*

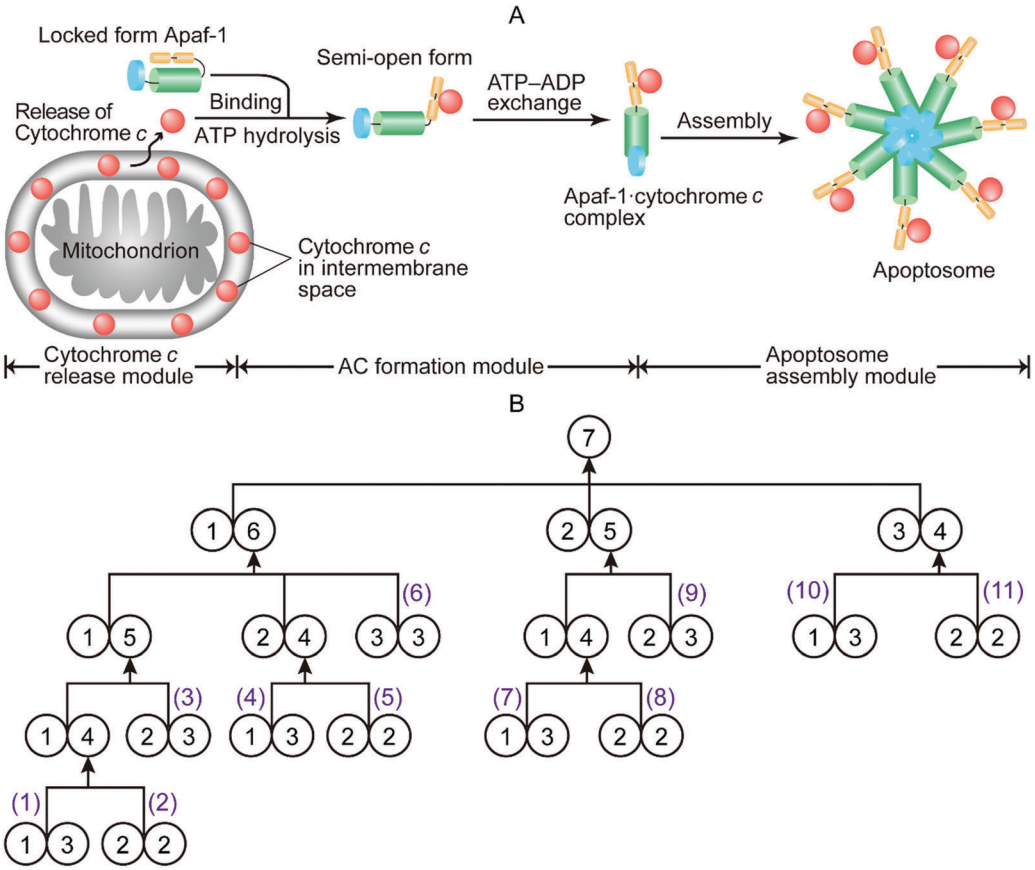

Fig. 1 Mechanism of apoptosome formation. (A) The model for apoptosome formation, which consists of three modules: cytochrome *c* release module, AC formation module, and apoptosome assembly module. (B) All 11 elementary routes for apoptosome assembly. The number *x* in a circle represents the oligomers composed of *x* molecules of AC, and number *i* in bracket represents the serial number of the route.

modules: cytochrome *c* release module, AC formation module, and apoptosome assembly module, as shown in Fig. 1A. In detail, Apaf-1 exists in a locked autoinhibited form typically in the absence of apoptotic stimuli. The apoptotic signal induces the release of mitochondrial cytochrome *c* into the cytosol. The binding of cytochrome *c* causes Apaf-1 to unfold partly, leading to a semi-open, still autoinhibited, form of Apaf-1. In order to be in an active form, Apaf-1 uses ATP hydrolysis and exchange to switch conformations. The activated Apaf-1 exists as a part of the AC complex. Seven molecules of AC oligomerize into a heptameric wheel-like apoptosome. All reactions are implemented as ordinary differential equations (ODEs), which are discussed in detail in the following sections.

2.1 Kinetics for cytochrome *c* release

The first landmark event in the intrinsic pathway is the release of cytochrome *c* from the mitochondria into the cytosol after exposure to apoptotic stimuli.[4] The release processes proceed fast and resemble asymmetric sigmoid traces that fit well to the mathematical behavior of a modified Gompertz function:[21]

$$[\mathrm{Cyt}\ c]_{\mathrm{m}}(t) = -a \times \mathrm{e}^{-\mathrm{e}^{-k_{\mathrm{d}}(t-t_{\mathrm{c}})}} + b. \qquad (1)$$

This function represents the concentration of cytochrome *c* in the mitochondria ($[\mathrm{Cyt}\ c]_{\mathrm{m}}$) with respect to time, where *a* and *b* denote the release amplitude and the total concentration of cytochrome *c*, respectively. k_{d} is the decay rate, and t_{c} the time of inflexion.[21] So the concentration of cytochrome *c* in the cytosol ($[\mathrm{Cyt}\ c]$) with respect to time is

$$[\mathrm{Cyt}\ c](t) = b - [\mathrm{Cyt}\ c]_{\mathrm{m}}(t) = a \times \mathrm{e}^{-\mathrm{e}^{-k_{\mathrm{d}}(t-t_{\mathrm{c}})}}. \qquad (2)$$

And the derivative of $[\mathrm{Cyt}\ c]$ is

$$\frac{\mathrm{d}[\mathrm{Cyt}\ c]}{\mathrm{d}t} = a \times k_{\mathrm{d}} \times \mathrm{e}^{-\mathrm{e}^{-k_{\mathrm{d}}(t-t_{\mathrm{c}})}} \times \mathrm{e}^{-k_{\mathrm{d}}(t-t_{\mathrm{c}})}. \qquad (3)$$

2.2 Formation of the Apaf-1·cytochrome *c* complex

Apaf-1 resides in the cytosol of healthy cells as a locked autoinhibited form.[16,22] When cytochrome *c* is released from the mitochondria into the cytoplasm, it binds to Apaf-1 and releases the lock, leading to a semi-open, still autoinhibited, form of Apaf-1.[16] The binding of Apaf-1 and cytochrome *c* is reversible and the formation of the complex ($\mathrm{Apaf}^{\mathrm{so}}$) is irreversible,[20]

$$\mathrm{Apaf} + \mathrm{Cyt}\ c \underset{k_1^-}{\overset{k_1^+}{\rightleftharpoons}} \mathrm{Apaf} : \mathrm{Cyt}\ c \xrightarrow{k_1^{\mathrm{c}}} \mathrm{Apaf}^{\mathrm{so}}.$$

Cytochrome *c* binding to Apaf-1 induces hydrolysis of the bound ATP (or dATP) to ADP (or dADP), which is subsequently replaced by exogenous ATP (or dATP).[23] In order to form the apoptosome,

Apaf-1 uses ATP (or dATP) hydrolysis and exchange to switch conformations. For simplicity, we implement dATP and ATP as one species, *i.e.*, ATP, and consider only the action of ATP on the formation of AC. The binding of ATP to Apaf^{so} is reversible and the formation of the stable AC complex is irreversible,

$$\mathrm{Apaf^{so}} + \mathrm{ATP} \underset{k_2^-}{\overset{k_2^+}{\rightleftharpoons}} \mathrm{Apaf^{so}:ATP} \overset{k_2^c}{\rightarrow} \mathrm{AC}.$$

Based on the law of mass action, the above two sets of biochemical reactions can be converted into seven ODEs,

$$\begin{aligned}
\frac{\mathrm{d[Apaf]}}{\mathrm{d}t} &= -k_1^+[\mathrm{Apaf}][\mathrm{Cyt}\ c] + k_1^-[\mathrm{Apaf:Cyt}\ c],\\
\frac{\mathrm{d[Cyt}\ c]}{\mathrm{d}t} &= -k_1^+[\mathrm{Apaf}][\mathrm{Cyt}\ c] + k_1^-[\mathrm{Apaf:Cyt}\ c],\\
\frac{\mathrm{d[Apaf:Cyt\ c]}}{\mathrm{d}t} &= k_1^+[\mathrm{Apaf}][\mathrm{Cyt}\ c] - (k_1^- + k_1^c)[\mathrm{Apaf:Cyt}\ c],\\
\frac{\mathrm{d[Apaf^{so}]}}{\mathrm{d}t} &= k_1^c[\mathrm{Apaf:Cyt}\ c] - k_2^+[\mathrm{Apaf^{so}}][\mathrm{ATP}]\\
&\quad + k_2^-[\mathrm{Apaf^{so}:ATP}],\\
\frac{\mathrm{d[ATP]}}{\mathrm{d}t} &= -k_2^+[\mathrm{Apaf^{so}}][\mathrm{ATP}] + k_2^-[\mathrm{Apaf^{so}:ATP}],\\
\frac{\mathrm{d[Apaf^{so}:ATP]}}{\mathrm{d}t} &= k_2^+[\mathrm{Apaf^{so}}][\mathrm{ATP}] - k_2^-[\mathrm{Apaf^{so}:ATP}]\\
&\quad - k_2^c[\mathrm{Apaf^{so}:ATP}],\\
\frac{\mathrm{d[AC]}}{\mathrm{d}t} &= k_2^c[\mathrm{Apaf^{so}:ATP}].
\end{aligned} \tag{4}$$

2.3 Apoptosome assembly

Once the AC monomer complexes (x_1) have been formed, they can self-assemble into different orders of oligomers, which finally form the heptameric apoptosome. For simplicity, we only consider the elementary reaction between two oligomers, one with i molecules of the AC complex (x_i) and another with j molecules (x_j), only when $i+j$ is no more than 7. For clarity, we first discuss the biochemical reactions where the produced oligomer can only dissociate into two oligomers that lead to its synthesis (*e.g.*, x_{1+4} dissociates into x_1 and x_4), which are called the elementary routes in the paper. Then we consider the reactions where the oligomer can dissociate into any allowed combinations, which are termed as the assembly pathways.

Like previous related considerations,[17,19,20,24] we assume that these reactions occur with a uniform association rate constant α and a uniform dissociation rate constant β, which are independent of the reactants. As a consequence, the reaction formula can be described as

$$x_i + x_j \underset{\beta}{\overset{\alpha}{\rightleftharpoons}} x_{i+j}, 1 \le i,j < i+j \le 7.$$

According to this formula, there are 11 possible elementary routes from the AC monomer complex to the heptamer apoptosome. The flow diagram of apoptosome assembly is shown in Fig. 1B.

The time variation of the concentration of each oligomer is determined by the term of production and consumption. In addition, the monomer is actually the individual AC complex. For simplicity, we denote x_i as the concentration of oligomer x_i, and x_i^{ss} as the steady state concentration of x_i in the equations. On the basis of the law of mass action, the general forms of the ODEs derived from the 11 elementary routes are given as

$$\begin{aligned}
\frac{\mathrm{d}x_1}{\mathrm{d}t} &= k_2^c[\mathrm{Apaf^{so}:ATP}]\\
&\quad - \alpha x_1(2x_1 + a_{12}x_2 + a_{13}x_3 + a_{14}x_4 + a_{15}x_5 + a_{16}x_6)\\
&\quad + \beta(2x_2 + a_{12}x_3 + a_{13}x_4 + a_{14}x_5 + a_{15}x_6 + a_{16}x_7),\\
\frac{\mathrm{d}x_2}{\mathrm{d}t} &= \alpha {x_1}^2 - \alpha x_2(a_{12}x_1 + a_{22}x_2 + a_{23}x_3 + a_{24}x_4 + a_{25}x_5)\\
&\quad + \beta(a_{12}x_3 + 2a_{22}x_4 + a_{23}x_5 + x_6 + x_7) - \beta x_2,\\
\frac{\mathrm{d}x_3}{\mathrm{d}t} &= a_{12}\alpha x_1x_2 - \alpha x_3(a_{13}x_1 + a_{23}x_2 + 2a_{33}x_3 + a_{34}x_4)\\
&\quad + \beta(a_{13}x_4 + a_{23}x_5 + 2a_{33}x_6 + x_7) - a_{12}\beta x_3,\\
\frac{\mathrm{d}x_4}{\mathrm{d}t} &= \alpha\left(a_{13}x_1x_3 + a_{22}{x_2}^2\right) - \alpha x_4(a_{14}x_1 + a_{24}x_2 + a_{34}x_3)\\
&\quad + \beta(a_{14}x_5 + a_{24}x_6 + a_{34}x_7) - \beta x_4(a_{13} + a_{22}),\\
\frac{\mathrm{d}x_5}{\mathrm{d}t} &= \alpha(a_{14}x_1x_4 + a_{23}x_2x_3) - \alpha x_5(a_{15}x_1 + a_{25}x_2)\\
&\quad + \beta(a_{15}x_6 + a_{25}x_7) - \beta x_5(a_{23} + a_{14}),\\
\frac{\mathrm{d}x_6}{\mathrm{d}t} &= \alpha\left(a_{15}x_1x_5 + a_{24}x_2x_4 + a_{33}{x_3}^2\right)\\
&\quad - \alpha a_{16}x_6x_1 + \beta a_{16}x_7 - \beta x_6(a_{15} + a_{24} + a_{33}),\\
\frac{\mathrm{d}x_7}{\mathrm{d}t} &= \alpha(a_{16}x_1x_6 + a_{25}x_2x_5 + a_{34}x_3x_4) - \beta x_7(a_{16} + a_{25} + a_{34}).
\end{aligned} \tag{5}$$

Here, the coefficients a_{ij} are either 1 or 0, representing if the oligomerization reaction between x_i and x_j occurs or not, respectively. For instance, if a_{23} is equal to 1, the oligomerization reaction between x_2 and x_3 occurs.

For an arbitrary given route, the related a_{ij} must be equal to 1, and the following five constraint equations can ensure that the unrelated a_{ij} are equal to 0,

$$a_{16} + a_{25} + a_{34} = 1, \tag{6}$$

$$a_{15} + a_{24} + a_{33} + a_{25} + a_{34} = 1, \tag{7}$$

$$a_{14} + a_{23} + a_{24} + a_{33} + a_{34} = 1, \tag{8}$$

$$a_{13} + a_{22} + a_{23} + a_{33} = 1, \tag{9}$$

$$a_{12} = \begin{cases} 1, \text{ if } a_{13} + a_{23} + a_{33} + a_{34} = 1 \\ 0, \text{ if } a_{13} + a_{23} + a_{33} + a_{34} = 0 \end{cases}. \tag{10}$$

The five equations are deduced from the topological structure in Fig. 1B. From top to bottom in Fig. 1B, the four layers represent the oligomerization between oligomeric species. Eqn (6) means

Table 1 List of initial conditions and parameters in the model

Symbol	Description	Value (unit)	Ref.
$[\text{Apaf}]_0$	Initial concentration of Apaf-1	0.3 (μM)	19
$[\text{Cyt } c]_0$	Initial concentration of cytochrome c in cytosol	0 (μM)	19
$[\text{ATP}]_0$	Initial concentration of ATP	10 (μM)	8
a	Release amplitude of cytochrome c (Cyt c)	3.8 (μM)	21
b	Total concentration of Cyt c	10 (μM)	19
k_d	Decay rate	1.65 (min^{-1})	21
t_c	Time of inflexion	2.5 (min)	21
k_1^+	Dimerization rate of Apaf-1 and Cyt c	0.24 (μM^{-1} min^{-1})	19
k_1^-	Dissociation rate of Apaf:Cyt c dimer	0.006 (min^{-1})	19
k_2^+	Dimerization rate of Apaf^{so} and ATP	0.1359 (μM^{-1} min^{-1})	19
k_2^-	Dissociation rate of Apaf^{so}:ATP dimer	0.1155 (min^{-1})	19
k_1^c	Transition rate from Apaf:Cyt c to Apaf^{so}	1 (min^{-1})	25
k_2^c	Transition rate from Apaf^{so}:ATP to AC	1 (min^{-1})	25
α	Association rate of oligomers	40 (μM^{-1} min^{-1})	19
β	Dissociation rate of oligomers	0.004 (min^{-1})	19

that there are three alternative ways to make the heptamer in the first layer. Eqn (7) is derived from the first and second layers to make sure that the three alternative ways producing the hexamer would not conflict with the two ways producing the heptamer (dimer plus pentamer and trimer plus tetramer). Eqn (8) is deduced from the first to third layers to show that only one of the five reactions exists in each elementary route. Eqn (9) has similar meaning as eqn (8). Eqn (10) is used to determine the value of a_{12}, which is 1 if the trimer exists for a certain route.

We now consider the biochemical reactions where the oligomer x_{i+j} can dissociate into two arbitrary oligomers (*e.g.*, x_5 dissociates into x_1 and x_4 or x_2 and x_3). As a result, all the assembly reactions are a combination of the 11 elementary routes. Thus, the total number of all possible assembly pathways is $\sum_{i=1}^{11} C_{11}^i = 2^{11} - C_{11}^0 = 2047$.

The initial conditions and parameters of the model are listed in Table 1. All the parameters are either extracted directly from experimental data or obtained from previously published models, with the cited references listed in the table.

2.4 Two criteria for optimal pathways

According to the literature,[19,26–28] we propose two criteria for the selection of the optimal assembly pathways: utilization rate and half-time. The utilization rate (U) is the conversion efficiency of the AC complex (x_1) into apoptosome (x_7),

$$U = \frac{7x_7}{\sum_{i=1}^{7} i \cdot x_i}. \quad (11)$$

Another similar concept is the proportion rate (P),[19] which is the proportion of the heptamer in all oligomers,

$$P = \frac{x_7}{\sum_{i=1}^{7} x_i}. \quad (12)$$

Although the definition of proportion rate is slightly different from the utilization rate, we prefer to employ utilization rate as a criterion, since it is more accurate in reflecting the assembly efficiency of apoptosome. Half-time is the time at which apoptosome production reaches its half maximum since the onset of cytochrome c release.

Because the formation of apoptosome must consume energy provided by the hydrolysis of ATP, a better assembly pathway should be with a higher utilization rate. A combined theoretical and experimental study revealed that the proportion of the heptamer in all oligomers is at least 60%, equivalent to the utilization rate of 65%.[19] Thus the first criterion is that the utilization rate should be no less than 65% for optimal pathways. Furthermore, kinetic analysis showed that the duration of cytochrome c release is approximately 5 min,[21,29] and that fully functional apoptosome should be assembled within 5–10 min after the completion of cytochrome c release.[19,26–28] So the second criterion is that the half-time should be shorter than 10 min for optimal pathways.

3 Results and discussion

To seek the optimal pathways for the assembly of apoptosome with the AC complex, we analyze mathematically the utilization rate of the 11 elementary routes and simulate computationally the properties of all 2047 possible pathways in the paper.

3.1 Mathematical analysis of utilization rate

First, we discuss the equilibrium states for the 11 elementary routes by setting the right hand of each equation of eqn (4) and (5) to 0. The last equation of eqn (4), that is, the first term of the first equation of eqn (5), is equal to 0. In this case, eqn (5) only include the variables for the seven oligomers, then the steady state equations of the 11 elementary routes have the following general form:

$$(x_2^{ss}, x_i^{ss}, x_7^{ss}) = (k(x_1^{ss})^2, a_i k^{i-1}(x_1^{ss})^i, k^6(x_1^{ss})^7). \quad (13)$$

Here $k = \alpha/\beta$, i = 3–6, and $a_i = 0$ if x_i is absent in a certain route. Moreover, a_i should satisfy the following two conditions: (1) a_3 and a_4 can't be 0 at the same time, since the trimer and the tetramer can't be absent for the heptamer-forming route at the same time; (2) at most two of the four coefficients of a_3, a_4, a_5,

and a_6 can be 0 for a given route, since no more than two different oligomers are allowed to be absent for a specific route.

During the process of apoptosome assembly, the total amount of Apaf-1 is consistently conserved. Then the utilization rate is given by

$$U = \frac{7k^6\left(x_1^{ss}\right)^7}{[\mathrm{Apaf}]_0}, \quad (14)$$

where $[\mathrm{Apaf}]_0$ is the initial concentration of Apaf-1. This conservation relation can also be expressed as

$$x_1^{ss} + 2k\left(x_1^{ss}\right)^2 + a_i\sum_{i=3}^{6} ik^{i-1}\left(x_1^{ss}\right)^i + 7k^6\left(x_1^{ss}\right)^7 = [\mathrm{Apaf}]_0. \quad (15)$$

Obviously, eqn (14) is a monotonically increasing function with respect to x_1^{ss}, so the bigger the x_1^{ss}, the higher the utilization rate.

Descartes' rule of signs indicates that eqn (15) has a unique positive root. Because k, which is equal to $\alpha/\beta = 10\,000\ \mu\mathrm{M}^{-1}$, is much larger than 1, we can infer from eqn (15) that the smaller the power number of k, the bigger the value of x_1^{ss} is. As a result, the utilization rates for 10th and 11th elementary routes are the highest, since they do not have pentamers and hexamers, *i.e.*, terms of k^5 and k^6. Although the above analysis is for individual elementary routes, the conclusion between the order of oligomer and the utilization rate is also valid for assembly pathways.

3.2 Mono-pathway with an individual elementary route

As a fact, each elementary route is a mono-pathway to assemble apoptosome. Thus, we numerically investigate the characteristics of the 11 mono-pathways, *i.e.*, the 11 elementary routes. Fig. 2A and B exhibit the time evolution of the concentrations of each oligomeric species for the 1st and 11th mono-pathways, respectively. The 1st mono-pathway reaches equilibrium more slowly than the 11th mono-pathway in which the half-time is less than 10 min. The 11 mono-pathways are not only different in dynamics but also in steady state concentration (Fig. 2C). The equilibrium concentrations of the heptamer for the 7th–11th mono-pathways are higher than those for the 1st–6th mono-pathways, with the 10th and 11th mono-pathways being the highest.

From Fig. 2A–C one can see that some oligomeric species are absent in some mono-pathways. For instance, the hexamer is absent in the 7th–11th mono-pathways, the pentamer absent in the 10th and 11th mono-pathways, and the tetramer absent in the 9th mono-pathway. As a result, the fewer the high-order oligomers (*i.e.*, tetramer, pentamer, and hexamer), the higher the equilibrium concentration of the heptamer.

Fig. 2D shows the proportion and utilization rate of the 11 mono-pathways. It can be seen that the utilization (or proportion) rates of the 4th–11th mono-pathways are above 65% (or 60%), which satisfy the first criterion of the optimal pathways. The half-times of the 11 mono-pathways are depicted in Fig. 2E.

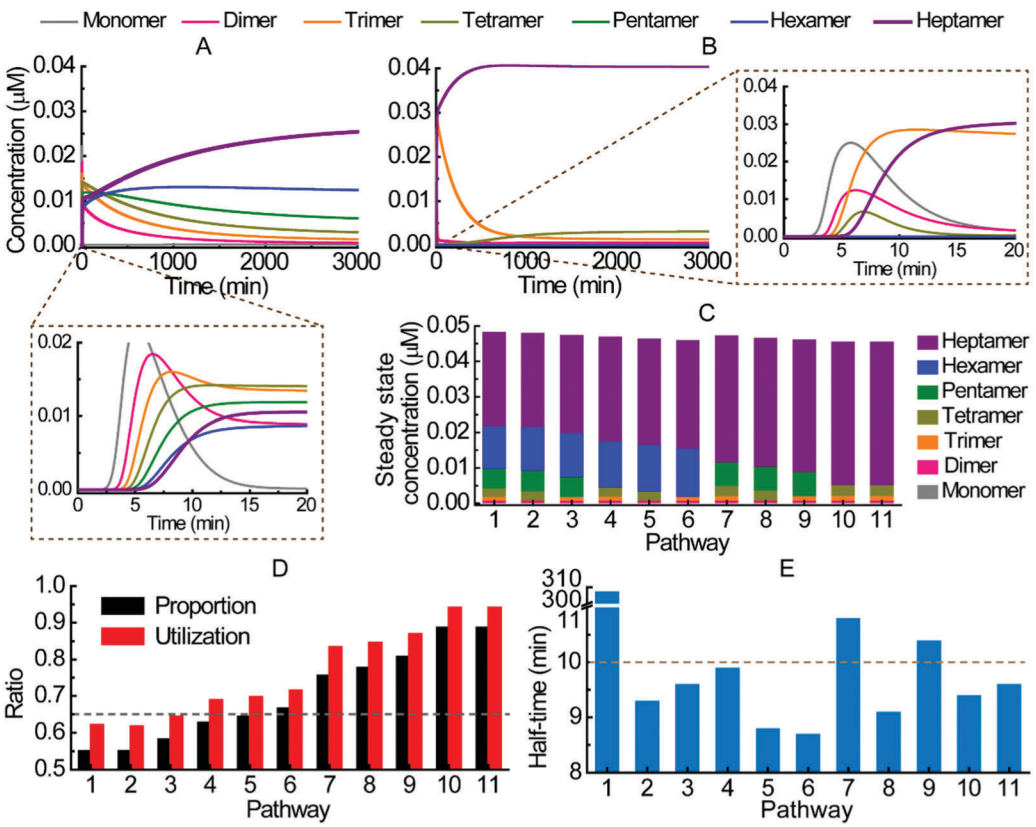

Fig. 2 The time course of (A) 1st and (B) 11th mono-pathways, with the enlarged parts during the first 20 min. (C) The equilibrium concentrations of each oligomers for each mono-pathway. (D) The proportion and utilization rates for each mono-pathway. (E) The half-time for each mono-pathway.

Except for the 1st, 7th, and 9th mono-pathways, the other mono-pathways have half-times less than 10 min, which satisfy the second criterion of the optimal pathways. Taken together, there are six optimal pathways in the 11 mono-pathways, *i.e.*, the 4th–6th, 8th, 10th, and 11th mono-pathways.

3.3 Bi-pathways combined with two elementary routes

Now, we systematically discuss the properties of bi-pathways which are combined with two elementary routes. There are $C_{11}^{2} = 55$ pathways with two elementary routes. The utilization rate and half-time for these 55 bi-pathways are plotted in Fig. 3A and B, respectively. Out of the 55 bi-pathways, there are 15 optimal pathways which are economical and fast relatively, with six optimal bi-pathways containing the 10th route, and five containing the 11th route.

3.4 Combinatorial pathways composed of multiple elementary routes

Then we select three representative examples to characterize the properties of the combination of multiple elementary routes. Fig. 4A–C display the time series of the concentrations of each oligomers for three combinatorial pathways: *i.e.*, the pathway with 1st–6th routes, the pathway with 7th–11th routes, and the pathway with all 11 routes, respectively. Compared to the other two combinatorial pathways, the combination pathway of all the 11 routes reaches equilibrium more quickly, suggesting that the combination possessing more pathways tends to have a shorter time required for achieving steady state.

Fig. 4D depicts the utilization rate and the half-time for the three combination pathways. It can be found that only the combination of the 7th–11th pathway meets the two criteria of the optimal pathway. The reaction scheme of the combination pathway of all 11 elementary routes was mainly considered in previous work.[17–19] Although the half-time of this scheme is the shortest, its utilization rate is lower than 65%.

3.5 The optimal pathways among all 2047 pathways

As a fact, we enumerate computationally all 2047 possible pathways to analyze the distributions of their utilization rates (Fig. 5A) and half-times (Fig. 5B). A small number of pathways (59 of 2047) have the utilization rates larger than 65%, while a large number of pathways (2037 of 2047) have the half-times smaller than 10 min. Thus, the utilization rate, rather than the assembly time, is the main criterion to determine the optimal pathways. In detail, the distribution of all 2047 data points (the 1st mono-pathway is not shown) is plotted in Fig. 5C, from which we can see that the selection of optimal pathways is a trade-off between efficiency and speed. The 52 optimal pathways are located at the top-left corner with red circles. Among these 52 points, there are 24 points at the most top-left corner plotted with open red circles, representing the best pathways for apoptosome assembly. The 52 optimal pathways comprising the 11 elementary routes are listed in detail in Table 2.

As a result, there are 52 optimal pathways satisfying the two criteria, as given in Fig. 6A. Their common features are illustrated in Fig. 6B and C. Fig. 6B displays the distribution of numbers of elementary routes to consist of these 52 optimal pathways. One can see that such numbers range only from one to five. In detail, the dominant optimal pathways are pathways with three elementary routes, followed by two and four. None of the optimal

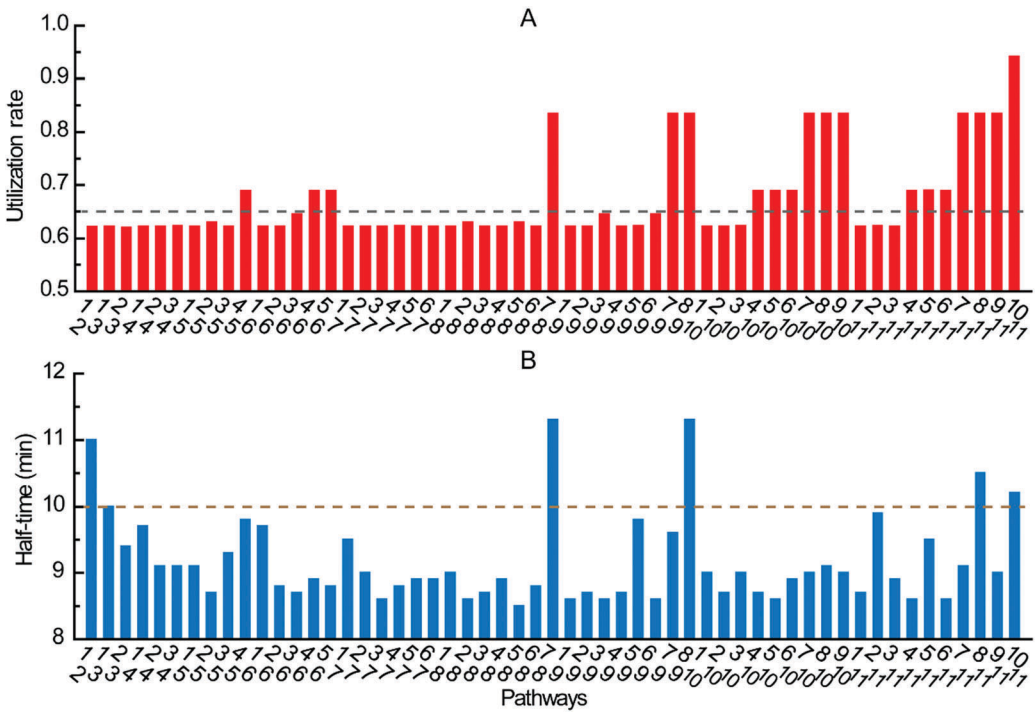

Fig. 3 The utilization rate (A) and half-time (B) of the 55 bi-pathways.

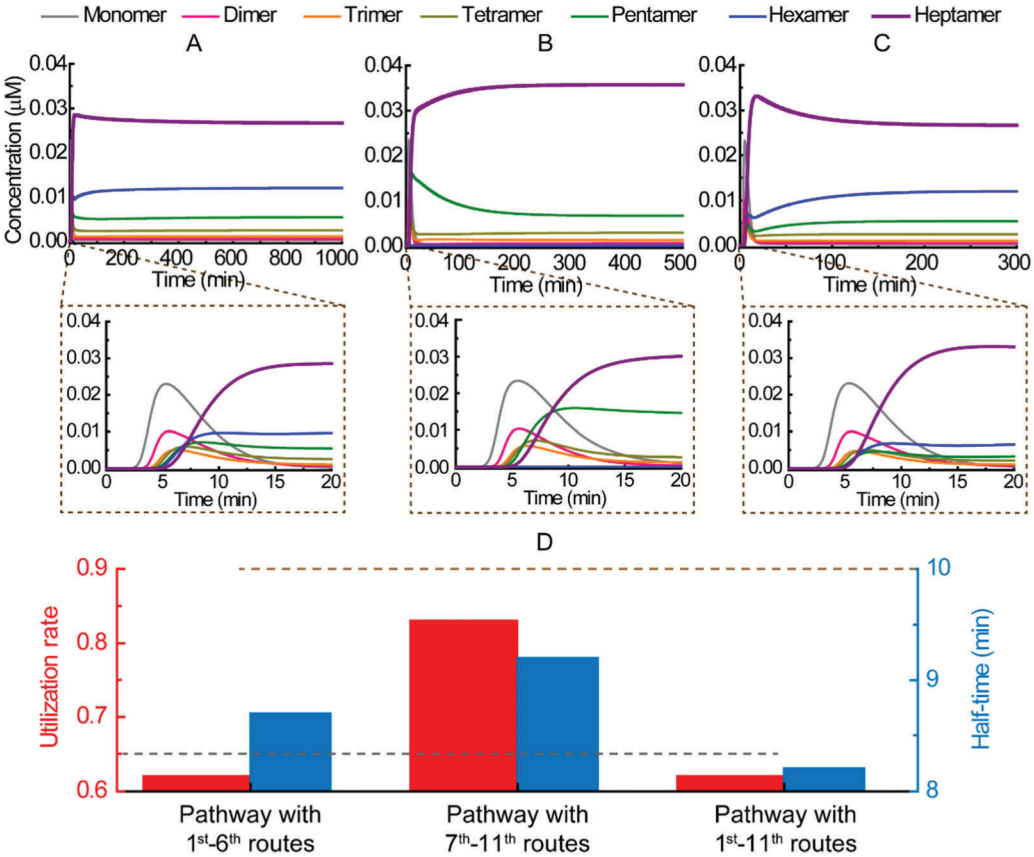

Fig. 4 Properties of three combinatorial pathways. (A–C) The time courses of the concentrations of each oligomer for the combination of 1st–6th, 7th–11th, and 1st–11th elementary routes, respectively, with the enlarged parts during the first 20 min. (D) The utilization rate (red column) and the half-time (blue column) for these three combination pathways.

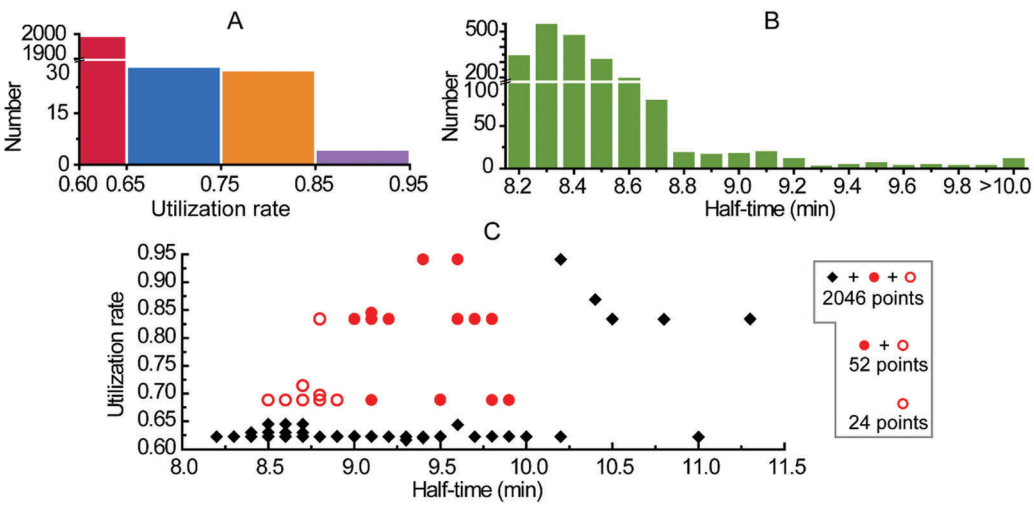

Fig. 5 The statistical properties of (A) utilization rate and (B) half-time of all 2047 pathways. (C) The distribution of 2046 pathways in the plane of half-time and utilization rate. Many points overlap with each other. The red circles represent the 52 optimal pathways, in which 24 best pathways at the most top-left corner are plotted with open red circles.

pathways possesses elementary routes more than five, indicating that it is not better with more elementary routes for assembly.

Fig. 6C plots the distribution of numbers of each elementary route counted in the 52 optimal pathways. In these 52 optimal pathways one could not find the 1st, 2nd, and 3rd elementary routes. Fig. 6C shows that the 10th and 11th elementary routes are most favorable for optimal pathways, followed by 4th, 5th, and 6th routes. This is consistent with the finding that the 4th,

Table 2 Results of the optimal pathways

ID	Routes occupied	Utilization (%)	Half-time (min)	ID	Routes occupied	Utilization (%)	Half-time (min)
1	4, 6, 10	69	8.5	27	9, 11	83	9.0
2	4, 6, 11	69	8.5	28	8	84	9.1
3	5, 6, 10	69	8.5	29	7, 11	83	9.1
4	5, 6, 11	69	8.5	30	8, 10	83	9.1
5	4, 5, 6, 10	69	8.5	31	7, 8,10	83	9.1
6	4, 5, 6, 11	69	8.5	32	7, 8, 11	83	9.1
7	4, 6, 10, 11	69	8.5	33	7, 10, 11	83	9.1
8	5, 6, 10, 11	69	8.5	34	8, 10, 11	83	9.1
9	4, 5, 6, 10, 11	69	8.5	35	7, 8, 10, 11	83	9.1
10	4, 11	69	8.6	36	4, 5, 6	69	9.1
11	5, 10	69	8.6	37	7, 9, 11	83	9.2
12	6, 11	69	8.6	38	8, 9, 10	83	9.2
13	4, 5, 10	69	8.6	39	7, 8, 9, 10	83	9.2
14	4, 5, 11	69	8.6	40	7, 8, 9, 11	83	9.2
15	4, 10, 11	69	8.6	41	7, 9, 10, 11	83	9.2
16	5, 10, 11	69	8.6	42	8, 9, 10, 11	83	9.2
17	4, 5, 10, 11	69	8.6	43	7, 8, 9, 10, 11	83	9.2
18	6	71	8.7	44	10	94	9.4
19	4, 10	69	8.7	45	5, 11	69	9.5
20	7, 9, 10	83	8.8	46	6, 10, 11	69	9.5
21	5	70	8.8	47	11	94	9.6
22	5, 6	69	8.8	48	7, 9	83	9.6
23	4, 6	69	8.9	49	8, 9, 11	83	9.7
24	6, 10	69	8.9	50	9, 10, 11	83	9.8
25	7, 10	83	9.0	51	4, 5	69	9.8
26	9, 10	83	9.0	52	4	69	9.9

The ID of pathway is ordered by the corresponding result of utilization-10 × half-time.

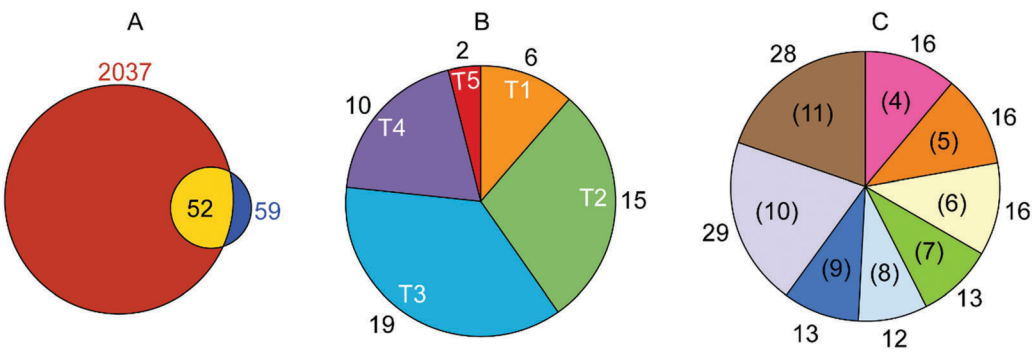

Fig. 6 The optimal 52 pathways. (A) The utilization rates of 59 pathways are >65%. The half-times of 2037 pathways are <10 min. There are 52 pathways satisfying both conditions. (B) The distribution of numbers of elementary routes consisting of these 52 optimal pathways. Here, T_x represents that there are x elementary routes in a combinatorial pathway. (C) The distribution of numbers of each individual elementary route counted in these 52 optimal pathways.

5th, 6th, 10th, and 11th elementary routes are the optimal mono-pathways.

4 Conclusions and perspectives

The assembly of apoptosome is a decisive point in the intrinsic pathway of apoptosis, because the accuracy of apoptosis depends significantly on how efficient and how quick the apoptosome is assembled.[17] However, the precise mechanism is obscure owing to the low stability of apoptosome, coupled with its large size and tendency to aggregate.[22] A more important question is that there should be some optimal pathways for the apoptosome assembly.

In order to address these questions, a dynamical model consisting of three modules has been proposed to integrate the biological information of apoptosome formation. By exhaustively analyzing all 2047 possible pathways, we find 52 pathways that optimally trade off efficiency and speed, which are also compatible with previous experimental measurements.[19,26–28] On the one hand, a combined theoretical and experimental study indicated that the utilization rate of the AC complex into apoptosome is at least 65%.[19] On the other hand, many experimental results suggested that fully functional apoptosome assembles within 10–15 min since the onset of cytochrome *c* release.[26–28]

According to these two criteria, we find 52 optimal pathways by our model. Rather than the assembly time, the utilization

rate is the main criterion to determine the optimal pathways. The dominant optimal pathways are pathways with three elementary routes, followed by two and four, which means that it is not better with more elementary routes for apoptosome assembly. The 10th and 11th elementary routes are the most favorable routes for optimal pathways, and more than half of the 52 optimal pathways possess these two elementary routes. One reason is that, as proved mathematically, the utilization rates for 10th and 11th elementary routes are the highest. Obviously, these two routes do not have pentamers and hexamers. In order to assemble the pentamers and hexamers, more monomers have to be consumed. As a result, the pentamers and hexamers cannot be easily converted into a heptamer due to the exhausted monomers in the system. Thus, the elementary routes with pentamer and hexamer typically present a low utilization rate. For another reason, the 10th and 11th elementary routes have the shortest steps to assemble into the apoptosome. Apparently, the shorter steps the elementary route has, the faster the reaction process will be. As a result, the 10th and 11th elementary routes have the fastest reaction time. Our conclusion is in accord with the evolutionary view that the natural selection often results in circuits with the smallest number of interactions.[30,31]

Most of the previous mathematical models on the intrinsic apoptotic pathway have handled the process of apoptosome assembly as a single nonlinear reaction term. Nakabayashi and Sasaki developed a model for this process by considering an assembly pathway comprising all 11 elementary routes.[17] Furthermore, they didn't take the effects of ATP (dATP) into account in the model. In fact, ATP (dATP) hydrolysis and exchange were thought to be the two required steps for apoptosome formation.[23,32] Their main conclusion is that the conversion efficiency of apoptosome assembly is maximized when the molar ratio of Apaf-1 to cytochrome *c* is 1 : 1.[17] However, it has been shown that the physiological concentration of cytochrome *c* is at least ten-folds that of Apaf-1.[19]

The heptameric apoptosome module discussed in the models in ref. 18 and 19 also followed the reaction scheme proposed by Nakabayashi and Sasaki with slight modifications. However, our discussion indicates that the reaction scheme with all 11 elementary routes for assembly has a low utilization rate. The reaction scheme considered by Ryu *et al.*[20] is the same as the 1st individual mono-pathway discussed in our work, which is the slowest pathway (Fig. 2) in all assembly pathways. In short, these aforementioned models cannot fully capture the comprehensive picture of apoptosome assembly.

Due to the lack of direct experimental evidence to reveal the association and dissociation dynamics in the process of apoptosome assembly, the proposed mechanism in the paper can only be considered as speculative. Nevertheless, our model predicts that the probability of occurrence of one mono-pathway may be scarce for apoptosome assembly, but the combinatorial pathways with the 10th and 11th elementary routes could be found more frequently. Further experiments are needed to ascertain the optimal pathways predicted by the model and to evaluate the physiological significance of the apoptosome assembly. In addition, because higher-order assemblies are prevalent in many biological processes,[33,34] the method in our paper is applicable to the other high-order aggregation systems, such as amyloid[34] and inflammasome,[35,36] and may provide insights into their assembly mechanisms.

Conflicts of interest

There are no conflicts to declare.

Acknowledgements

We acknowledge support from the National Natural Science Foundations of China (Grant No. 11504214, 11675134, and 31370830), and the 111 Project (Grant No. B16029).

References

1 R. C. Taylor, S. P. Cullen and S. J. Martin, *Nat. Rev. Mol. Cell Biol.*, 2008, **9**, 231.
2 S. W. Tait and D. R. Green, *Nat. Rev. Mol. Cell Biol.*, 2010, **11**, 621–632.
3 J. Plati, O. Bucur and R. Khosravi-Far, *Integr. Biol.*, 2011, **3**, 279–296.
4 S. G. Kruglik, B.-K. Yoo, J.-C. Lambry, J.-L. Martin and M. Negrerie, *Phys. Chem. Chem. Phys.*, 2017, **19**, 21317–21334.
5 E. N. Shiozaki, J. Chai and Y. Shi, *Proc. Natl. Acad. Sci. U. S. A.*, 2002, **99**, 4197–4202.
6 X. Teng and J. M. Hardwick, *Cell*, 2010, **141**, 402–404.
7 Y. Shi, *Cell*, 2004, **117**, 855–858.
8 P. Li, D. Nijhawan, I. Budihardjo, S. M. Srinivasula, M. Ahmad, E. S. Alnemri and X. Wang, *Cell*, 1997, **91**, 479–489.
9 H. Zou, W. J. Henzel, X. Liu, A. Lutschg and X. Wang, *Cell*, 1997, **90**, 405–413.
10 H. Zou, Y. Li, X. Liu and X. Wang, *J. Biol. Chem.*, 1999, **274**, 11549–11556.
11 D. Acehan, X. Jiang, D. G. Morgan, J. E. Heuser, X. Wang and C. W. Akey, *Mol. Cell*, 2002, **9**, 423–432.
12 M. Zhou, Y. Li, Q. Hu, X.-C. Bai, W. Huang, C. Yan, S. H. Scheres and Y. Shi, *Genes Dev.*, 2015, **29**, 2349–2361.
13 T. C. Cheng, C. Hong, I. V. Akey, S. Yuan and C. W. Akey, *Elife*, 2016, **5**, e17755.
14 Q. Hu, D. Wu, W. Chen, Z. Yan, C. Yan, T. He, Q. Liang and Y. Shi, *Proc. Natl. Acad. Sci. U. S. A.*, 2014, **111**, 16254–16261.
15 Y. Li, M. Zhou, Q. Hu, X.-C. Bai, W. Huang, S. H. Scheres and Y. Shi, *Proc. Natl. Acad. Sci. U. S. A.*, 2017, **114**, 1542–1547.
16 S. J. Riedl and G. S. Salvesen, *Nat. Rev. Mol. Cell Biol.*, 2007, **8**, 405–413.
17 J. Nakabayashi and A. Sasaki, *J. Theor. Biol.*, 2006, **242**, 280–287.
18 H. A. Harrington, K. L. Ho, S. Ghosh and K. Tung, *Theor. Biol. Med. Modell.*, 2008, **5**, 26.
19 M. L. Würstle and M. Rehm, *J. Biol. Chem.*, 2014, **289**, 26277–26289.
20 S. Ryu, S.-C. Lin, N. Ugel, M. Antoniotti and B. Mishra, *Syst. Synth. Biol.*, 2008, **2**, 49–66.

21 M. Rehm, H. J. Huber, C. T. Hellwig, S. Anguissola, H. Dussmann and J. H. Prehn, *Cell Death Differ.*, 2009, **16**, 613.
22 S. Yuan and C. W. Akey, *Structure*, 2013, **21**, 501–515.
23 H.-E. Kim, F. Du, M. Fang and X. Wang, *Proc. Natl. Acad. Sci. U. S. A.*, 2005, **102**, 17545–17550.
24 E. J. Deeds, J. A. Bachman and W. Fontana, *Proc. Natl. Acad. Sci. U. S. A.*, 2012, **109**, 2348–2353.
25 J. G. Albeck, J. M. Burke, S. L. Spencer, D. A. Lauffenburger and P. K. Sorger, *PLoS Biol.*, 2008, **6**, e299.
26 M. M. Hill, C. Adrain, P. J. Duriez, E. M. Creagh and S. J. Martin, *EMBO J.*, 2004, **23**, 2134–2145.
27 D. Twiddy, D. G. Brown, C. Adrain, R. Jukes, S. J. Martin, G. M. Cohen, M. MacFarlane and K. Cain, *J. Biol. Chem.*, 2004, **279**, 19665–19682.
28 P. Saikumar, M. Mikhailova and S. L. Pandeswara, *Front. Biosci.*, 2007, **12**, 3343–3354.
29 J. Goldstein, C. Munoz-Pinedo, J. Ricci, S. Adams, A. Kelekar, M. Schuler, R. Tsien and D. Green, *Cell Death Differ.*, 2005, **12**, 453–462.
30 T. Friedlander, A. E. Mayo, T. Tlusty and U. Alon, *PLoS One*, 2013, **8**, e70444.
31 M. Adler, P. Szekely, A. Mayo and U. Alon, *Cell Syst.*, 2017, **4**, 1–11.
32 Q. Bao and Y. Shi, *Cell Death Differ.*, 2007, **14**, 56–65.
33 H. Wu, *Cell*, 2013, **153**, 287–292.
34 H. Wu and M. Fuxreiter, *Cell*, 2016, **165**, 1055–1066.
35 J. Chai and Y. Shi, *Natl. Sci. Rev.*, 2014, **1**, 101–118.
36 V. A. Rathinam and K. A. Fitzgerald, *Cell*, 2016, **165**, 792–800.